Journal of The Electrochemical Society, **154** (6) A542-A546 (2007)
0013-4651/2007/154(6)/A542/5/$20.00 © The Electrochemical Society

Rate Characteristics of Anatase TiO_2 Nanotubes and Nanorods for Lithium Battery Anode Materials at Room Temperature

Jinyoung Kim and Jaephil Cho*,z

Department of Applied Chemistry, Kumoh National Institute of Technology, Gumi, Korea 730-701

Anatase TiO_2 nanotubes and nanorods were prepared by annealing mixed $H_2Ti_2O_5 \cdot H_2O$ and anatase TiO_2 nanotubes at 300 and 400°C, respectively. The first discharge capacities of anatase nanotubes and nanorods were 296 mAh/g ($Li_{0.88}TiO_2$) and 215 mAh/g ($Li_{0.64}TiO_2$), respectively. Irreversible capacity ratios were 14 and 15% for anatase nanotubes and nanorods, respectively. Capacity retention of the nanotubes was 81%, and that of the nanorods was 40% after 30 cycles. In contrast to nanotubes, the high rate performance of nanorods strongly depended on the electrode density of the electrode. Nanorods with 0.5 g/cm^3 (=12 mg/cm^2) showed 200 and 160 mAh/g at 0.5 and 10 C rates, respectively. However, nanotubes showed no capacity decrease at 0.5 or 10 C under an electrode density of either 1 or 0.5 g/cm^3. Under 2 g/cm^3 (=31 mg/cm^2), nanotubes showed 245 and 185 mAh/g at 0.5 and 2 C rates, respectively.
 [DOI: 10.1149/1.2724756]

Manuscript submitted November 30, 2006; revised manuscript received February 7, 2007. Available electronically April 11, 2007.

Recently, TiO_2 materials have been studied for use in applications that require high rate performance. TiO_2(B), anatase, and rutile TiO_2 have been intensively investigated.[1-8] In general, the uptake of Li^+ has been found to be much better in anatase lattice than in rutile structures. The anatase structure has a tetragonal body-centered space group $I4_1/1md$, and the structure comprises TiO_6 octahedra sharing two adjacent edges with two other octahedra so that infinite planar double chains are formed.[9] Diffusion of Li ions in an anatase framework occurs along a reaction path connecting the octahedral interstitial sites. However, when $x = 0.5$ ($Li_{0.5}TiO_2$), the symmetry of the unit cell decreases from the original $I4_1/1md$ to the orthorhombic $Pmn2_1$ space group symmetry due to loss of symmetry in the y direction.[10] The change in symmetry is accompanied by a decrease of the unit cell along the c axis and an increase along the b axis, resulting in an increase of ~4% of the unit cell volume. However, a 4% increase leads to rapid capacity fade.[3]

For chemical intercalation with n-butyllithium in bulk TiO_2, $x = 0.7$ seems to be the most reliable value. However, for electrochemical experiments, $x = 0.5$ is most consistently reported as the maximum insertion ratio.[11] Repulsive Coulombic interactions between lithium ions are expected to be responsible for lithium content to $x = 0.7$. Li surface storage on nanometer-sized particles can be energetically more favorable than bulk insertion. TiO_2-B nanotubes can store Li in $Li_{1.01}TiO_2$-B (corresponding to a specific discharge capacity of 338 mAh/g at first cycling) but show an irreversible capacity ratio of 24%.[1] Gao et al. reported that anatase nanotubes with 10–15 nm outer diameters and 200–400 nm lengths are prepared by annealing the hydrothermally prepared protonated nanotubes at 500°C in an argon atmosphere.[12] These nanotubes show first discharge and charge capacities of 340 and 200 mAh/g, respectively. Li et al. reported that anatase TiO_2 nanotubes with outer diameters of 9 nm and several hundred nanometer lengths were prepared by annealing at 350°C using hydrothermal-treated protonated titanate nanotubes.[13] The first discharge and charge capacities were 314 and 248 mAh/g, respectively, in the loading of the active material of 3–4 mg/cm^2. However, for the actual application of the materials, the loading of the active material is too low. Unfortunately, except for Li's work, all previous papers related to TiO_2 did not report the loading condition of the electrode (electrode density), even though rate performance is significantly affected by electrode density.

In this study, we prepared anatase nanotubes that were several micrometers long and had outer diameters of ~7.5 nm. High rate performance is reported at different electrode density conditions up to 2 g/cm^3 (=31 mg/cm^2). We also compared TiO_2 nanorods with tubes at the same loading conditions.

Experimental

Anatase TiO_2 nanotubes were first reported by Kasuga et al. in the reaction of TiO_2 particles with a NaOH aqueous solution.[14,15] When bulk anatase TiO_2 is treated in 10 M NaOH at 120°C, layered-structured titanates such as $Na_xTi_yO_z$ can be formed as intermediate products. During the hydrothermal process, Na^+ cations residing between edge-shared TiO_6 octahedral layers can be replaced gradually by H_2O molecules.[16,17] Intercalated H_2O molecules are larger than Na^+ ions, so the interlayer distance increases and the static interaction between neighboring TiO_6 octahedral sheets weakens. Consequently, layered titanate particles exfoliate to form nanosheets that curl up from the edges to form TiO_2 nanotubes.[18-20]

The TiO_2 source used for preparing the nanotubes was commercially available rutile TiO_2 powder (particle size 0.3 μm). A mixture of 4 g of TiO_2 powder, 70 mL NaOH, and distilled water was treated with ultrasonication for 30 min, followed by treatment at 150°C in a Teflon-lined autoclave for 48 h. After treatment, the sample was treated with a 0.1 M HCl solution and dried at 100°C for 12 h. The dried sample was annealed further at 300 and 400°C for 3 h.

High-resolution transmission electron microscopy (HRTEM) samples were prepared by evaporation of the samples in acetone or hexane on carbon-coated copper grids. The field-emission electron microscope was a JEOL 2010F operating at 200 kV. Powder X-ray diffraction (XRD) measurements were carried out using a Rigaku DMax/2000PC with a Cu-target tube. Nitrogen adsorption isotherms were obtained with a Micrometrics ASAP 2020 system, and samples were degassed for 24 h at 150°C before measurements were taken.

Cathodes for the battery test cells were made of nanotube or nanorod materials, Super P carbon black, and polyvinylidene fluoride (PVDF) binder (Solef) in a weight ratio of 80:10:10. The slurry was prepared by thoroughly mixing an N-methyl-2-pyrrolidone (NMP) (Aldrich) solution of PVDF, carbon black, and the cathode material. Electrode density was controlled by changing the electrode coating thickness. Electrode density was calculated based upon the total amounts of electrode compositions and was converted to the amount of active material per cm^2 in the electrode. Coin-type half-cells (2016R size), prepared in a helium-filled glove box, contained TiO_2, a Li metal anode, a microporous polyethylene separator, and an electrolyte solution of 1 M $LiPF_6$ in ethylene carbonate/dimethyl carbonate (EC/DMC) (1:1 vol %) (Cheil Industries, Korea).

* Electrochemical Society Active Member.
z E-mail: jpcho@kumoh.ac.kr

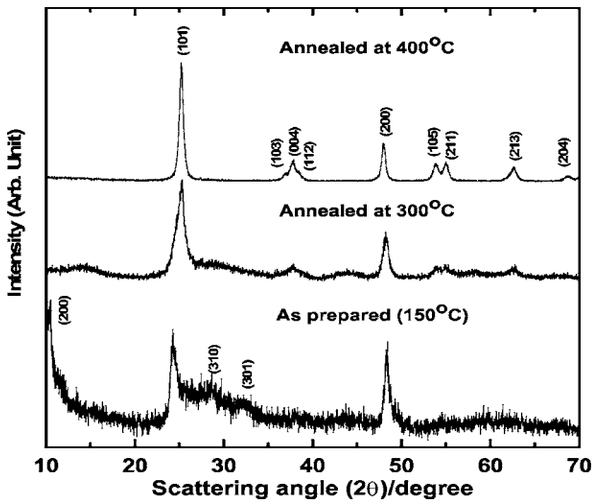

Figure 1. XRD patterns of as-prepared nanotubes at 150°C, nanotubes annealed at 300°C, and nanotubes annealed at 400°C.

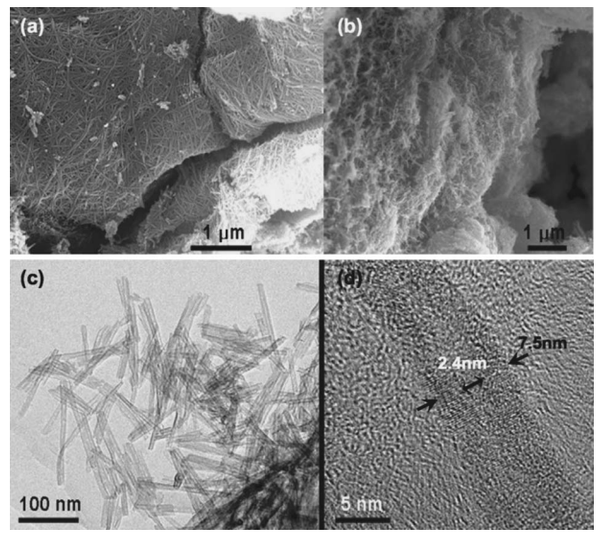

Figure 2. SEM and TEM images of as-prepared nanotubes at 150°C: (a, b) SEM top and side views of the nanotubes, respectively, (c) TEM images, and (d) a HRTEM image of (c).

Results and Discussion

Figure 1 shows XRD patterns of the as-prepared titanate nanotubes and nanotubes annealed at 300 and 400°C for 3 h in air. The XRD pattern of peaks in the as-prepared samples (150°C) is matched with anatase TiO_2 phase and layered $H_2Ti_2O_5{\cdot}H_2O$ phase [(200), (310), and (301) miller indices].[21] $H_2Ti_2O_5{\cdot}H_2O$ is a product of $Na_2Ti_2O_5$ and has a monoclinic lattice, with parallel kinked layers of edge-sharing TiO_6 octahedra. Such layers intercalate alkali metal cations, M^+, which can be further ion-exchanged with H^+ to produce protonic hydrous titanates, $H_2Ti_2O_5{\cdot}H_2O$. The reaction is topotactic; hence, the protonic titanates preserve the original layered structure. However, thermal dehydration of protonic titanates leads to TiO_2 while the anatase or rutile phases grow, depending on the pretreatment conditions. Wang et al. reported mixed anatase and TiO_2(B) nanotubes annealed at 350°C using 30% rutile and 70% anatase TiO_2 in a 60 mL solution of 20 M NaOH(aq) and ethanol.[6] However, Gao et al. reported that $H_2Ti_3O_7$ nanotubes convert into anatase TiO_2 nanotubes at 500°C in an argon atmosphere, but products consisted of mostly tubes and a few rods.[12]

Figure 2 shows scanning electron microscopy (SEM; a and b are top and side views, respectively) and transmission electron microscopy (TEM; c and d) images of the titanate nanotubes obtained from the hydrothermal treatment of rutile particles with 10 M NaOH at 150°C for 48 h. Figure 2d is an enlarged image of Fig. 2c. The as-prepared nanotubes were open-ended, several micrometers long, and possessed inner and outer diameters of 2.4 and 7.5 nm, respectively. Figure 3a and b shows TEM images of the sample after annealing at 300°C. Inner and outer diameters were 3 and 7.2 nm, respectively. Figure 3c and d shows TEM images of as-prepared nanotubes that were annealed at 400°C for 2 h. These images show the formation of nanorods due to corruption of the nanotubes. The magnified lattice image clearly shows the lattice fringe of (101) planes corresponding to 3.57 Å of anatase TiO_2.

As-prepared TiO_2 and annealed TiO_2 nanotubes at 300°C were characterized by nitrogen adsorption at 77 K, and the nanotubes show typical IV-type isotherm curves in Fig. 4. An adsorption and desorption hysteresis loop gradually increased up to P/Po $\approx$ 0.4 and exhibited an abrupt increase in the high-pressure region at P/Po $>$ 0.8. This can be associated with capillary condensation and multilayer adsorption of nitrogen in the mesopores. Pore size of the as-prepared and annealed samples was 2.7 and 3.1 nm, which are similar values observed in TEM results, indicating the formation of nanotubes with mesopores. The specific surface areas determined by Brunauer-Emmett-Teller (BET) measurements of as-prepared and annealed samples were 213 and 239 m^2/g, respectively. An increased BET surface area was due to the removal of H_2O from $H_2Ti_2O_5{\cdot}H_2O$ in the phase. Mesopore volumes of as-prepared and annealed samples were 1.3 and 1.7 cm^3/g, respectively. Nanotubes with higher surface areas likely lead to higher electrode/electrolyte contact areas. This coupled with shorter diffusion paths into the lattices and reduced strain of intercalation may lead to improved cycling performance compared to nanorods. Nanotubes needed intercalation of only 25–30 Å. BET surface area of the annealed sample at 400°C (nanorods) was 100 m^2/g.

Figure 5 shows voltage profiles of nanotubes annealed at 300°C and the corresponding ex situ XRD patterns at different cutoff voltages (A-I). Diffraction peaks were very broad because of the nanoscale dimension of the nanotubes. There were no changes in the diffraction patterns on intercalation and deintercalation on the first

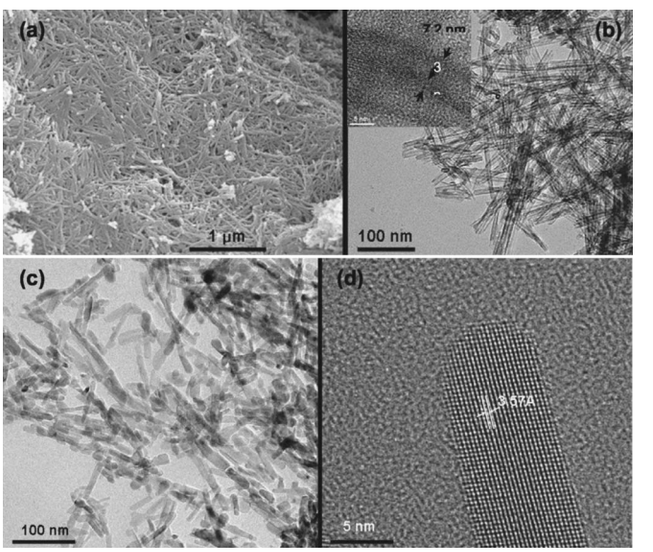

Figure 3. SEM (a) and TEM images of nanotubes annealed at 300°C (b) and nanorods (c and d). (b) An enlarged TEM image of (a), and (d) an enlarged image of (c).

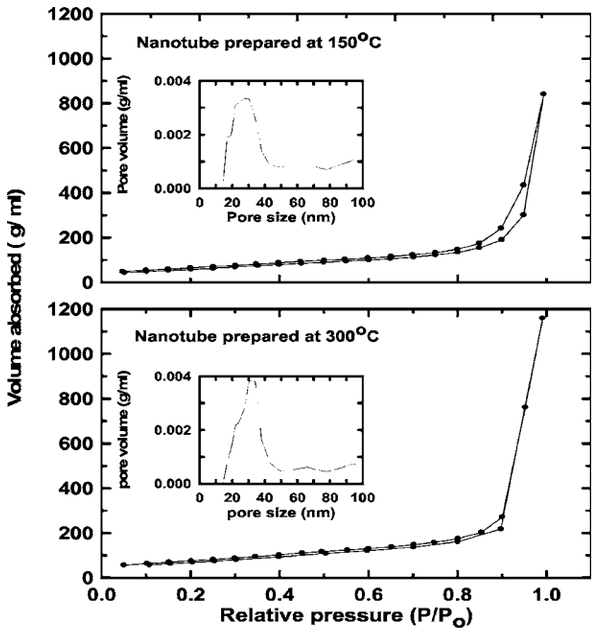

Figure 4. Nitrogen adsorption and desorption isotherms of the as-prepared and annealed nanotube (300°C) at 77 K. Corresponding Barrett-Joyner-Halenda plots are shown in the insets.

cycling, except for a slight shift of the peaks to higher scattering angles, corresponding to a slight lattice expansion on intercalation, which was reversible on deintercalation. These results show that there was no significant structural change.

Figure 6 shows cycling profiles of as-prepared and annealed samples and nanorods between 2.5 and 1 V at a rate of 0.1 C (=25 mA/g) under an electrode density of 2 g/cm^3 (=31 mg/cm^2).

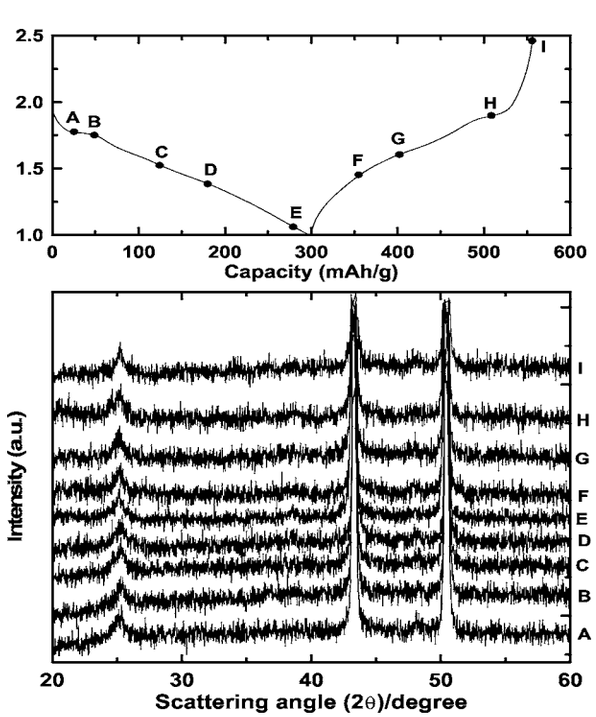

Figure 5. Voltage profiles of the anatase nanotubes and corresponding ex situ XRD patterns of annealed nanotubes at designated cutoff voltages.

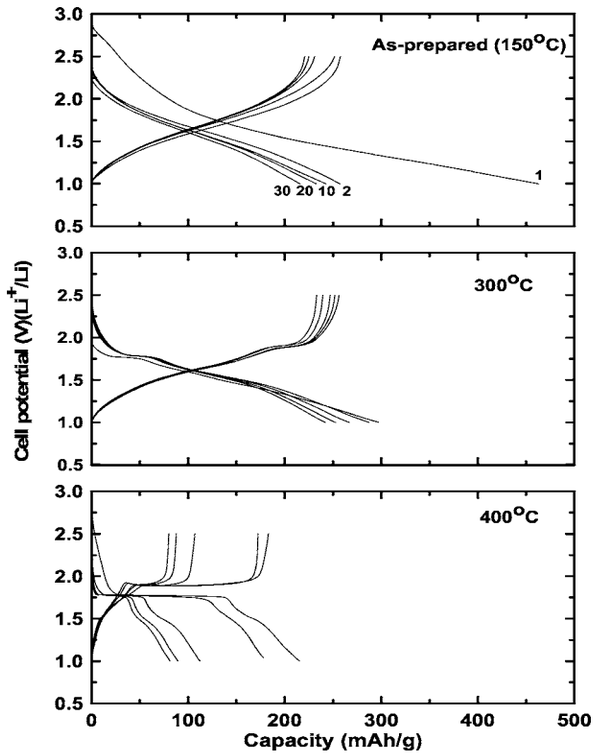

Figure 6. Voltage profiles of the as-prepared (150°C), annealed nanotubes (300°C), and nanorods (400°C) between 2.5 and 1 V at a rate of 0.1 C (=25 mA/g) after 1st, 2nd, 10th, 20th, and 30th cycles using coin-type half-cells (electrode density was 2 g/cm^3).

As-prepared nanotubes (150°C) showed a large irreversible capacity of 218 mAh/g with a reversible capacity of 245 mAh/g. The large irreversible capacity was due to the decomposition of water molecules at low voltages. Upon subsequent cycling, irreversible capacity was not observed, indicating that water was completely consumed during the first discharge process. Because the as-prepared sample had mixed phases of $H_2Ti_2O_5 \cdot H_2O$ and TiO_2, Li ions may be partially inserted into the $H_2Ti_2O_5$ nanotubes according to the reaction: $xLi^+ + H_2Ti_2O_5 \leftrightarrow Li_xH_{2-x}Ti_2O_5^{x(n-1)+} + xH^+$. Capacity retention after 30 cycles was 47% at the rate of 0.1 C (=25 mA/g), but capacity retention between the 2nd and 30th cycles was 84%. However, this material cannot be used for practical application to Li-ion cells due to a high irreversible capacity. However, nanotubes annealed at 300°C had first discharge and charge capacities of 297 and 256 mAh/g, respectively, and showed a 14% irreversible capacity. The capacity retention after 30 cycles was 81%. Due to the decreased surface area of the nanorods, the first discharge capacity decreased to 215 mAh/g with a subsequent charge capacity of 183 mAh/g. The irreversible capacity ratio was 15%. At the same electrode density conditions as the other samples, the nanorod capacity retention after 30 cycles was 40%.

In Fig. 6, the plateau at ~1.75 V becomes less resolved with decreasing annealing temperatures because of the distribution in compositions arising from the preferential intercalation of smaller particles.[1,6] For nanorods, a more pronounced plateau was observed. The appearance of the plateau indicated a more ordered TiO_2 crystal structure, thus leading to a more ordered first-order phase transition from Li_xTiO_2 to $Li_{0.5}TiO_2$.[9] Generally, such phase transitions cause local variations in strain associated with the 4% increase of the cell volume upon intercalation. Well-developed two-phase regions can result in more lattice strain during lithium-ion reactions compared to nanotubes, and therefore induce faster capacity fading.[22] However,

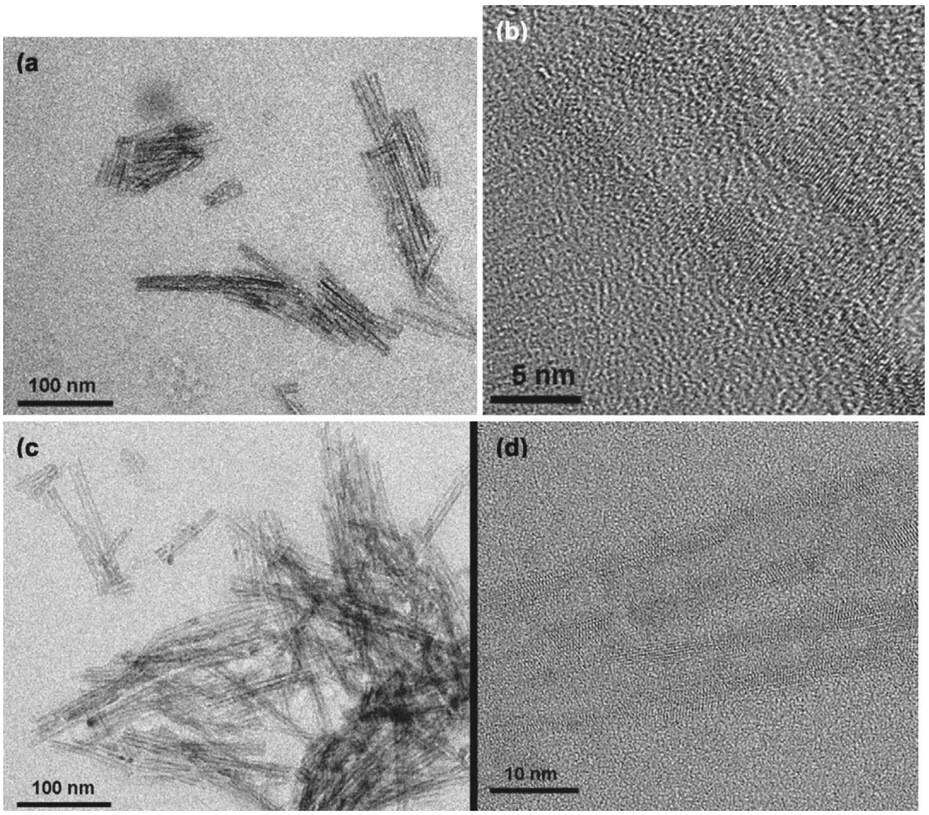

Figure 7. TEM images of the as-prepared at 150°C (a,b) and annealed nanotubes at 300°C (c,d) after 30 cycles.

smoothing of the profile may represent a different lithium insertion mechanism into TiO_2 for nanorods. This voltage profile changes may associate with dimensional confinement of the TiO_2 nanostructure, thus changing the Li ion insertion energetics. Such changes in energetics could originate from the contribution of surface free energy to the overall Li insertion process, as well as differences in the structural strains associated with lithium insertion/extraction or differences in Li^+/e^- ordering, compared with the nanorods.[1,6] TiO_2 nanotubes held the curved nanosheet-like morphology with thin wall structures and high surface areas. Consequently, they can accommodate Li ions through a different mechanism than nanorods. In addition, increasing the specific surface area induced a substantial capacitive contribution to the overall capacity. Figure 7 depicts TEM images of the as-prepared and annealed nanotubes after 30 cycles. For as-prepared nanotubes at 150°C, the outer diameter expanded to ~10 from ~7.5 nm. The annealed nanotubes at 300°C appeared to maintain the outer diameter before cycling, but both samples showed no structural damages.

Figure 8 shows the voltage profiles of samples annealed at 300 and 400°C with increasing C rates from 0.5, 1, 5, and 10 C under an electrode density of 2 g/cm^3 (charge rate was fixed at 0.1 C). Nanotubes annealed at 300°C showed improved capacity retention relative to as-prepared samples. At the 5 and 10 C rates, the annealed nanotubes showed capacity retentions of 205 and 180 mAh/g, respectively (retention ratio was 74%). However, nanorods exhibited faster capacity decay than nanotubes annealed at 300°C. The first discharge capacity was 178 mAh/g at the 0.5 C rate, but the capacity decreased to 110 mAh/g at the 10 C rate (retention ratio was 62%). Such a rapid capacity fading may be related to high electrode density in which the electrode was so densely packed that the pore fraction available for the electrolyte to be absorbed decreased. Contact area between active material and electrolytes decreased.

To investigate the rate capability of nanotubes and nanorods, electrode density was varied from 0.5 to 2 g/cm^3 (12–31 mg/cm^2). To our knowledge, there are no systematic studies of the loading level of the TiO_2 with electrochemical results. Only one study reported the lading level for testing TiO_2, and the first discharge and charge capacities of the TiO_2 were 314 and 248 mAh/g, respectively, in the loading of the active material of 3–4 mg/cm^2.[13] Figure 9 shows the rate performance of nanotubes annealed at 300°C and nanorods at different C rates with various electrode densities. Nanorods showed improved capacity and capacity retention at higher C rates with decreasing electrode densities from 2 to 0.5 g/cm^3. Ca-

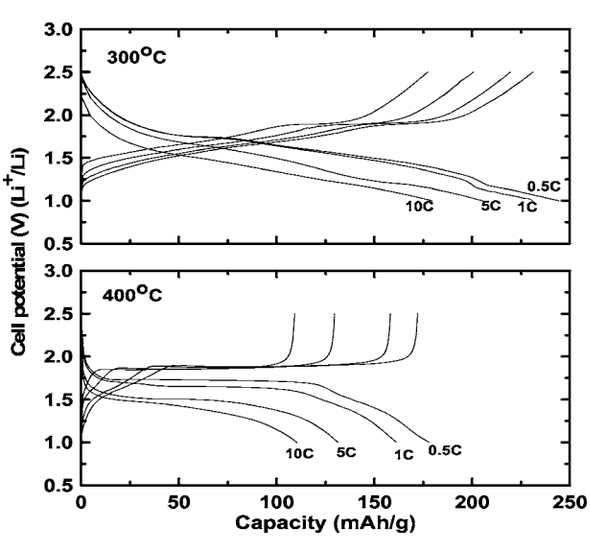

Figure 8. Rate capabilities of the annealed nanotubes (annealed at 300°C) and nanorods (annealed at 400°C) between 2.5 and 1 V at rates of 0.5, 1, 5, and 10 C using coin-type half-cells (charge rate was fixed at 0.1 C (=25 mA/g) and electrode density was 2 g/cm^3).

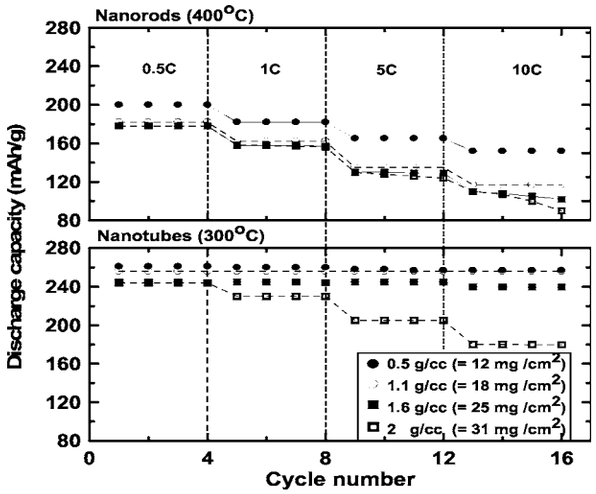

Figure 9. Plot of rates vs discharge capacity in annealed nanotubes (annealed at 300°C) and nanorods (annealed at 400°C) with different C rates. Discharge rates were 0.5, 1, 5, and 10 C using coin-type half-cells between 2.5 and 1 V.

pacity improved by 69% from 90 to 152 mAh/g at the 10 C rate upon the 4th cycling when electrode density decreased from 2 to 0.5 g/cm^3. This result indicates that loosely packed composite electrodes enhanced the contact areas with the electrolytes. Similar trends were observed in nanotubes, but no capacity fading was observed at 0.5 or 1 g/cm^3, even under 10 C rate cycling. At present, the loading level of natural graphite in commercial 18650R cells with a capacity of 2600 mAh is 1.6 g/cm^3; therefore, our loading levels of the TiO_2 are not a low value and in our case, when the loading level was increased above 2 g/cm^3, the copper foil was found to be severely deformed. Because the aim of this study is to investigate the rate characteristics of anatase TiO_2 nanotubes and nanorods at room temperature, we did not further investigate the temperature affect. However, we are planning to carry out studies of the temperature effect of the TiO_2 nanotubes and nanorods on the rate performances at various temperature ranges.

Conclusions

TiO_2 nanotubes obtained hydrothermally at 150°C had mixed phases of $H_2Ti_2O_5$ and anatase TiO_2. These nanotubes had a reversible capacity of 218 mAh/g with an irreversible capacity ratio of 47%. However, annealed nanotubes showed higher BET surface areas than as-prepared samples and had a reversible capacity of 296 mAh/g with a significantly decreased irreversible capacity of 14%. Lowering the crystallite size had a beneficial effect on the cyclability of these materials by accommodating structural changes better during the electrochemical process. Nanotubes exhibited excellent high rate performances even at an electrode density of 2 g/cm^3. Capacity retention at the 10 C rate was 74%, compared to the 0.5 C rate. At relatively low electrode densities, such as 0.5 g/cm^3, no capacity fade was observed even at a 10 C rate.

Acknowledgment

This research was financially supported by Ministry of Commerce, Industry, and Energy (MOCIE) and Korea Industrial Technology Foundation (KOTEF) through the Human Resource Training Project for Regional Innovation.

Kumoh National Institute of Technology assisted in meeting the publication costs of this article.

References

1. G. Armstrong, A. R. Armstrong, J. Canales, R. Garcia, and P. G. Bruce, *Electrochem. Solid-State Lett.*, **9**, A139 (2006).
2. Y.-S. Hu, L. Kienle, Y.-G. Guo, and J. Maier, *Adv. Mater. (Weinheim, Ger.)*, **18**, 1421 (2006).
3. G. Sudant, E. Baudrin, D. Larcher, and J.-M. Tarascon, *J. Mater. Chem.*, **15**, 1263 (2005).
4. I. Moriguchi, R. Hidaka, H. Yamada, T. Kudo, H. Murakami, and N. Nakashima, *Adv. Mater. (Weinheim, Ger.)*, **18**, 69 (2006).
5. A. R. Armstrong, G. Armstrong, J. Canales, R. Garcia, and P. G. Bruce, *Adv. Mater. (Weinheim, Ger.)*, **17**, 862 (2005).
6. Q. Wang, Z. Wen, and J. Li, *Inorg. Chem.*, **45**, 6944 (2006).
7. T. Ohzuku, T. Kodama, and T. Hirai, *J. Power Sources*, **14**, 153 (1985).
8. L. Kavan, M. Kalbáč, M. Zukalová, I. Exnar, V. Lorenzen, R. Nesper, and M. Graetzel, *Chem. Mater.*, **16**, 477 (2004).
9. M. Marketa, M. Kalbáč, L. Kavan, I. Exnar, and M. Graetzel, *Chem. Mater.*, **17**, 1248 (2005).
10. R. J. Cava, D. W. Murphy, S. Zahurak, A. Santoro, and R. S. Roth, *J. Solid State Chem.*, **53**, 64 (1984).
11. M. Wagemaker, R. van de Krol, A. P. M. Kentgens, Ad A. Van Well, and F. M. Mulder, *J. Am. Chem. Soc.*, **123**, 11454 (2001).
12. X. P. Gao, Y. Lan, H. Y. Zhu, J. W. Liu, Y. P. Ge, F. Wu, and D. Y. Song, *Electrochem. Solid-State Lett.*, **8**, A26 (2005).
13. J. Li, Z. Tang, and Z. Zhang, *Electrochem. Solid-State Lett.*, **8**, A316 (2005).
14. T. Kasuga, M. Hiramatsu, A. Hoson, T. Sekino, and K. Niihara, *Adv. Mater. (Weinheim, Ger.)*, **11**, 1307 (1999).
15. T. Kasuga, M. Hiramatsu, A. Hoson, T. Sekino, and K. Niihara, *Langmuir*, **14**, 3160 (1998).
16. M. Wei, Y. Konishi, H. Zhou, H. Sugihara, and H. Arakawa, *Solid State Commun.*, **133**, 493 (2005).
17. D. V. Bavykin, J. M. Friedrich, and F. C. Walsh, *Adv. Mater. (Weinheim, Ger.)*, **18**, 1 (2006).
18. Q. Chen, G. H. Du, S. Zhang, and L.-M. Peng, *Acta Crystallogr., Sect. B: Struct. Sci.*, **B58**, 587 (2002).
19. T. P. Feist and P. K. Davies, *J. Solid State Chem.*, **101**, 275 (1992).
20. X. Sun and Y. Li, *Chem.-Eur. J.*, **9**, 2229 (2003).
21. J.-N. Nian and H. Teng, *J. Phys. Chem. B*, **110**, 4193 (2006).
22. R. van de Krol, A. Goosens, and E. A. Meulenkamp, *J. Electrochem. Soc.*, **146**, 3150 (1999).